Topochemical Fluorination of La2NiO4+d:

Wissel, Kerstin; Heldt, Jonas; Groszewics, Pedro; Dasgupta, Supratik; Breitzke, Hergen; Donzelli, Manuel; Waidha, Aamir; Fortes, Andrew; Rohrer, Jochen; Slater, Peter; Buntkowsky, Gerd; Clemens, Oliver

DOI:
10.1021/acs.inorgchem.8b00661

Topochemical Fluorination of La_2NiO_{4+d}: Unprecedented ordering of oxide and fluoride ions in $La_2NiO_3F_2$

Journal:	*Inorganic Chemistry*
Manuscript ID	ic-2018-006616.R2
Manuscript Type:	Article
Date Submitted by the Author:	17-Apr-2018
Complete List of Authors:	Wissel, Kerstin; TU Darmstadt, Institut für Materialwissenschaft, Fachgebiet Materialdesign durch Synthese Heldt, Jonas ; TU Darmstadt, Institut für Materialwissenschaft, Fachgebiet Materialdesign durch Synthese Groszewicz, Pedro; Eduard-Zintl Institut for Inorganic and Physical Chemistry, AK Buntkowsky Dasgupta, Supratik; Technische Universität Darmstadt, Institut für Materialwissenschaft, Fachgebiet Dünne Schichten Breitzke, Hergen; Friedrich-Schiller-Universität Jena, Technische Universität Darmstadt Donzelli, Manuel; Technische Universitat Darmstadt, Institut für Materialwissenschaft, Fachgebiet Materialdesign durch Synthese Waidha, Aamir Iqbal; Technische Universitat Darmstadt, Material Science Fortes, Andrew Dominic; ISIS Facility, Rutherford Appleton Laboratory Rohrer, Jochen; Materialmodellierung, Materialwissenschaft Slater, Peter; University of Birmingham, School of Chemistry Buntkowsky, Gerd; Technische Universität Darmstadt , Eduard-Zintl Institute for Physical and Inorganic Chemistry Clemens, Oliver; Technische Universitat Darmstadt, Institut für Materialwissenschaft, Fachgebiet Materialdesign durch Synthese; University of Birmingham, School of Chemistry; Karlsruher Institut für Technologie, Institut für Nanotechnologie

Topochemical Fluorination of La_2NiO_{4+d}: Unprecedented ordering of oxide and fluoride ions in $La_2NiO_3F_2$

Kerstin Wissel[a], Jonas Heldt[a], Pedro B. Groszewicz[b], Supratik Dasgupta[c], Hergen Breitzke[b], Manuel Donzelli[a], Aamir I. Waidha[a], Andrew Dominic Fortes[d], Jochen Rohrer[e], Peter R. Slater[f], Gerd Buntkowsky[b], Oliver Clemens[a,f,g,*]

[a] Technische Universität Darmstadt, Institut für Materialwissenschaft, Fachgebiet Materialdesign durch Synthese, Alarich-Weiss-Straße 2, 64287 Darmstadt, Germany

[b] Technische Universität Darmstadt, Institut für Physikalische Chemie, Alarich-Weiss-Straße 8, 64287 Darmstadt, Germany

[c] Technische Universität Darmstadt, Institut für Materialwissenschaft, Fachgebiet Dünne Schichten, Alarich-Weiss-Straße 2, 64287 Darmstadt, Germany

[d] ISIS Facility, Rutherford Appleton Laboratory, Harwell Science and Innovation Campus, Didcot, Oxfordshire OX11 0QX, United Kingdom

[e] Technische Universität Darmstadt, Institut für Materialwissenschaft, Fachgebiet Materialmodellierung, Otto-Berndt-Straße 3, 64287 Darmstadt, Germany

[f] University of Birmingham, School of Chemistry, Birmingham B15 2TT, United Kingdom

[g] Karlsruher Institut für Technologie, Institut für Nanotechnologie, Hermann-von-Helmholtz-Platz 1, 76344 Eggenstein-Leopoldshafen, Germany

* Corresponding Author

Fax: +49 6151 16 21991

E-Mail: oliver.clemens@md.tu-darmstadt.de

Abstract

The Ruddlesden-Popper (K_2NiF_4) type phase $La_2NiO_3F_2$ was prepared via a polymer based fluorination of La_2NiO_{4+d}. The compound was found to crystallize in the orthorhombic space group *Cccm* (a = 12.8350(4) Å, b = 5.7935(2) Å, c = 5.4864(2) Å). This structural distortion results from an ordered half occupation of the interstitial anion layers, and has not been observed previously for K_2NiF_4-type oxyfluoride compounds. From a combination of neutron and X-ray powder diffraction, and ^{19}F MAS NMR spectroscopy, it was found that the fluoride ions are only located on the apical anion sites, whereas the oxide ions are located on the interstitial sites. This ordering results in a weakening of the magnetic Ni-F-F-Ni superexchange interactions between the perovskite layers, and a reduction of the antiferromagnetic ordering temperature to 49 K. Below 30 K, a small ferromagnetic component could be found, which may be the result of a magnetic canting within the antiferromagnetic arrangement, and will be the subject of a future low-temperature neutron diffraction study. Additionally, DFT based calculations were performed in order to further investigate different anion ordering scenarios.

Keywords

Oxyfluorides; Ruddlesden-Popper; Perovskites; Fluorination; La_2NiO_{4+d}; Magnetism

1 Introduction

Compounds with Ruddlesden-Popper type structure $A_{n+1}B_nO_{3n+1}$ are known for a variety of functional properties, among them superconductivity [1-5], catalytic [6], ferroelectric [7] and magnetic [8-9] properties. The member with n = 1 (A_2BX_4, often referred to as K_2NiF_4 type structure) can be understood as being build-up of alternating layers of perovskite ABX_3 and rock salt AX layers. The highest symmetry of this arrangement is *I*4/*mmm*. In this arrangement, two crystallographically distinguishable oxide ion sites exist, which are the so-called equatorial (X1, 4*c*) and apical (X2, 4*e*) anion site (Figure 1). Furthermore, depending on the transition metal B involved, many Ruddlesden-Popper type compounds possess a certain flexibility to become significantly oxidized. This originates from the presence of large interstitial anion sites (X3, 4*d*) within the rock salt type layers (Figure 1). If all those interstitial sites are filled by oxide ions, one usually talks about the Aurivillius type structure, as found, e.g., for Bi_2WO_6 [10].

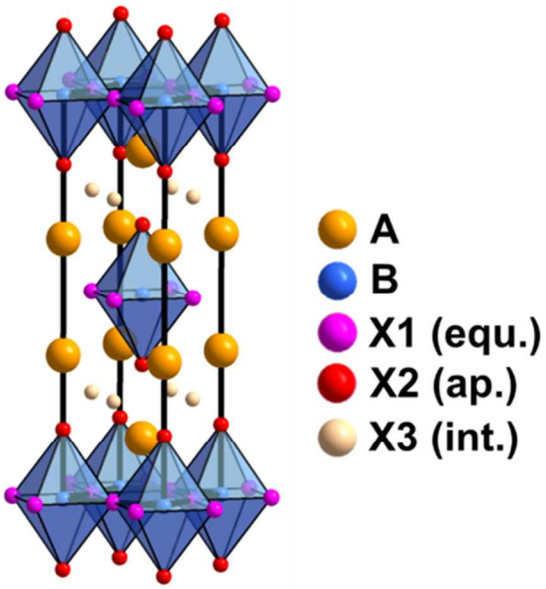

Figure 1. Schematic drawing of the n = 1 Ruddlesden-Popper type (K_2NiF_4 type) structure with composition $A_2B(X1_{equatorial})_2(X2_{apical})_2(X3_{inerstitial})_2$. Equatorial, apical and interstitial anion sites are shown with different colors.

For Ruddlesden-Popper type compounds, the interstitial anion sites can also be filled with high amounts of fluoride ions [11-13]. This can result in strong changes of the above-mentioned functional properties and further has led to the development of intercalation based electrode materials for fluoride ion batteries [14-15]. In previous reports, it was found that the fluoride ions show a predominant occupation of the interstitial site in case the composition allows for occupation of the apical and equatorial sites by oxide ions only, i.e., for compositions $A_2BO_xF_y$ with $x \geq 4$ (e.g. for $LaSrMnO_4F_{1.7}$ and $La_2CoO_4F_{1.2}$ [14-15]). For x = 2 and $(x+y) \leq 4$, the fluoride ions are located only on interstitial anion sites (e.g. $Sr_2CuO_2F_2$ [16-17], $Ca_2CuO_2F_2$ [18], $Ca_{2-x}Sr_xCuO_2F_2$ [18]

or $Ba_{2-x}Sr_xPdO_2F_2$ (Nd_2CuO_4 type (T'-type) structure) [19]). Occupation of both, the apical and the interstitial sites, can be found for $2 < x < 4$ and $(x+y) > 4$ (e.g. for $Sr_2CuO_2F_{2+\delta}$ (La_2CuO_4 type (T-type) structure with additional fluoride ions δ on interstitial anion sites) [4], $Ca_2CuO_2F_{2+\delta}$ (Nd_2CuO_4 type (T'-type) structure with additional fluoride ions δ on anion apical sites) [20] or $Sr_2TiO_3F_2$ [21-22]). Fluorinated compounds with significant occupancy of the interlayers were found to show a strong expansion of the unit cell perpendicular to the plane of the interlayers, where the filling of the interlayers can occur in a staged ($LaSrMnO_4F$ [23-24] and $Sr_2TiO_3F_2$ [21-22]) or a statistical manner (e.g. $Ba_2ZrO_3F_2(H_2O)_{0.5}$ [25] or $LaSrMnO_4F_{1.7}$ [15]). A half-filled ordered scenario of fluoride ions is further known for the n = 2 compound $Sr_3Fe_2O_4F_4$ [26].

In this article, we report on the preparation of $La_2NiO_3F_2$ via polymer-based low-temperature fluorination of La_2NiO_{4+d}. For the structural characterization a coupled analysis of X-ray and neutron powder diffraction data, in combination with ^{19}F MAS NMR and DFT based analysis was performed. We show that $La_2NiO_3F_2$ possesses half filling of every interlayer in an ordered fashion, which results in a unique orthorhombic structural distortion without strong expansion perpendicular to the interlayers, which was previously unknown for oxyfluorides. Even more fascinating, this distortion results in an unexpected ordering of the anions, with the oxide ions being located at the equatorial and interstitial sites and the fluoride ions being located on the apical sites. The fluorination results in a strong decrease of the magnetic ordering temperature from 330 K for La_2NiO_{4+d} [27] to 49 K, which is explained by a decrease of the Ni-F-F-Ni superexchange interaction strength between the perovskite layers via the apical fluoride ions.

2 Experimental

2.1 Synthesis

The precursor oxide $La_2NiO_{\mathbf{4+d}}$ was synthesized by a solid-state reaction between dried (700 °C, 4 h) La_2O_3 (Alfa Aesar, 99.9%) and NiO (Alfa Aesar, 99%). Stoichiometric amounts of the starting materials were mixed using a ball mill (300 RPM, 1 h), and twice heated to 1200 °C for 12 h in air with an intermediate regrinding. For the topochemical fluorination of $La_2NiO_{\mathbf{4+d}}$ to $La_2NiO_3F_2$, the oxide was mixed with the fluorination agent polyvinylidene fluoride CH_2CF_2 (PVDF, Sigma-Aldrich) [22] with 2.5 % excess and heated to 370 °C for 24h under air.

$Sr_2TiO_3F_2$ and $Sr_2TiO_3FH_{0.48}$ were used as reference materials to support the NMR analysis of $La_2NiO_3F_2$. $Sr_2TiO_3F_2$ was prepared via topochemical fluorination of Sr_2TiO_4 at 370 °C using PVDF. $Sr_2TiO_3FH_{0.48}$ was prepared by mixing $Sr_2TiO_3F_2$ with NaH in a 1:1 molar ratio and heating at 300 °C for 48 h in a stainless steel vacuum tight reactor. More details about those compounds can be found in Slater et al.[21-22] and Wissel et al.[21, 28].

2.2 Characterization

X-ray diffraction (XRD) patterns were recorded on a Bruker D8 Advance in Bragg-Brentano geometry with Cu K_α radiation and a VANTEC detector. The high quality data for the Rietveld refinement of $La_2NiO_3F_2$ were recorded using a variable divergence slit of 4 mm with measurement times of 17 h for the angular range of 5 to 130°. High-temperature XRD patterns were recorded on the same setup (fixed divergence slit of 0.3°) using an Anton Paar HTK 1200N high-temperature chamber in the angular range between 20° and 47° with a scan time of ~ 0.5 h.

Time-of-flight (TOF) powder neutron diffraction (NPD) data were recorded on the HRPD high-resolution diffractometer at the ISIS pulsed spallation source (Rutherford Appleton Laboratory, U.K.) [29-30]. ~ 1.5 g of $La_2NiO_3F_2$ were loaded into a 6 mm diameter thin-walled, cylindrical vanadium sample can, and data were collected at ambient temperature for ~ 20 μAh proton beam current to the ISIS target (corresponding to ~ 0.5 h beam time). The time-of-flight data were normalized to the incident spectrum and corrected for detector efficiency by reference to a V:Nb standard using the Mantid suite of diffraction utilities [31].

Analysis of diffraction data were performed using the Rietveld method with the program TOPAS V. 5.0 [32-33] using the whole 2θ-range as well as the data recorded on all the diffraction banks of the TOF diffractometer. The instrumental intensity distribution of the XRD and NPD instruments was determined empirically from a sort of fundamental parameters set [34] using a reference scan of LaB_6 (NIST 660a) and silicon, respectively. The microstructural parameters (crystallite size and strain broadening) were refined to adjust the peak shapes. Different isotropic thermal parameters were refined for the different crystallographic sites.

The average oxidation states of Ni of La_2NiO_{4+d} and $La_2NiO_3F_2$ were determined by iodometric titrations. Samples (~ 50 mg) were dissolved in 1 M HCl containing an excess of KI. Starch solution was added as an indicator. Titration was performed using a standardized $Na_2S_2O_3$ solution with a concentration of 0.01 mol/l. The average oxidation state was determined on three independent measurements.

The surface oxidation state of Ni was examined by X-ray photoelectron spectroscopy (XPS) analysis on a Physical Electronic VersaProbe XPS unit (PHI 5000 spectrometer) with Al K_α radiation (1486.6 eV). All detail spectra were recorded with a step size of 0.1 eV and a pass energy of 23.5 eV. A neutralizer compensated surface charge effects by using low energy electrons and Ar^+ ions. The binding energies were calibrated to the gold $4f_{7/2}$ ($Au4f_{7/2}$) and silver $3d_{5/2}$ ($Ag3d_{5/2}$) emission line at 84 eV and 368 eV. To determine the integral intensity and the

exact binding energies of the emission lines, the spectra were background corrected according to Shirley [35].

Magnetic characterization was performed with a Quantum Design MPMS. Powder samples were contained in gelatin capsules and mounted in a straw. Zero-field cooled (ZFC) and field-cooled (FC) curves were measured from 5 K to 350 K in the applied field $\mu_0 H$ = 1T. All magnetization measurements were corrected by the diamagnetic contributions of the phases which are present in the phase mixtures as well as by contribution stemming from gelatin capsule and straw used for sample mounting [36].

^{19}F MAS NMR spectra were recorded in a magnetic field of 14.1 T with a Bruker Avance III spectrometer at a frequency of 564.686388 MHz. An 1.3 mm MAS HX probe was employed with spinning frequencies between 10 kHz and 55 kHz. Paramagnetic compounds were diluted with inert substances in powder form to prevent any complications when spinning the ZrO_2 rotors. Spectra of $Sr_2TiO_3F_2$ and $Sr_2TiO_3FH_{0.48}$ were recorded with a single pulse experiment with a 90 degree pulse length of 2.1 us and a recycle delay of 2 s and 10 s, respectively. The number of scans varied from 16 to 128, according to the dilution of the sample. Baseline correction was performed with cubic-splines. The ^{19}F MAS NMR spectra of $La_2NiO_3F_2$ were recorded with a Hahn-echo, with pulse length of 2.1 for the $\pi/2$ and 4.2 us for π pulses. The echo delay was rotor synchronized and set to one rotor period. A total of 512 scans were accumulated with a recycle delay of 0.1 s. Full echoes were processed, spectra are displayed in magnitude mode to prevent phasing errors. The ^{19}F chemical shift scale was referenced to $CFCl_3$ at 0 ppm using the resonance of PTFE at -123.4 ppm as an external standard.[37]

2.3 DFT+U Calculations

Density functional theory (DFT) calculations were performed using the projector-augmented wave (paw) method [38] as implemented in the planewave code VASP 5.3.5 [39]. For exchange and correlation the parametrization of Perdew, Burke and Ernzerhof (PBE) [40-41] was used. To correct for the strong localization of d-electrons in Ni, a sphericaly averaged Hubbard correction (DFT+U) [42-43] was applied. In accordance with previous calculations [44-45] on compounds containing divalent nickel, a value of U_{eff} = U-J = 5 eV was chosen. In all calculations we use a planewave cutoff of 500 eV and a Γ-centered 4 x 8 x 8 Monkhorst-Pack k-point mesh.

Electronic self-consistency is considered to be reached as total energies vary by less 10^{-6} eV in consecutive iterations. Full structure optimizations (atomic positions and unit-cell vectors) were performed until forces did not exceed a value of 0.001 eV/Å.

By increasing the k-mesh to 6 x 12 x 12, we have checked that the calculated energy differences are converged to ~ 0.002 eV per formula unit of $La_2NiO_3F_2$.

3 Results and Discussion

3.1 Structural and Compositional Characterization of $La_2NiO_3F_2$

The fluorination of La_2NiO_{4+d} was examined for a variety of different molar ratios x of La_2NiO_{4+d}:CH_2CF_2 (PVDF), with x between 0.5 and 2. A nearly single phase product was obtained using only marginal (~ 2 %) excess relative to stoichiometric ratios of La_2NiO_{4+d} to PDVF (x = 1:1). For lower fluorine contents (x = 2:1), a two phase mixture of the unreacted tetragonal parent phase La_2NiO_{4+d} and the phase obtained when using a stoichiometric ratio (x = 1:1) were found, whereas for higher amounts of PVDF (x = 1:1.5, 1:2), again the phase obtained when using a stoichiometric ratio (x = 1:1) and LaF_3 were found. The amount of LaF_3 increased with increasing amounts of polymer used.

In order to determine the composition of the product obtained for x = 1, the compound was further investigated using iodometric titration and XPS (Figure 2). While titration provides the bulk oxidation state of Ni, XPS is only surface sensitive. The titration of La_2NiO_{4+d} and $La_2NiO_3F_2$ indicated average Ni oxidation states of Ni^{2+} in both compounds (+2.10(1) for La_2NiO_{4+d} (d ~ 0.05) and +2.06(1) for $La_2NiO_3F_2$). Therefore, a small reduction of the oxidation state is found, and this has been observed previously for PVDF based fluorinations even in air, e.g., the synthesis of $SrFeO_2F$ from $SrFeO_{3-d}$ [46-47]. For XPS, due to a partial overlap of the Ni $2p_{3/2}$ and the La $3d_{3/2}$ peaks, the Ni 3p peak was used to investigate the Ni valence; note that the $3p_{1/2}$ and $3p_{3/2}$ peaks are in general not well resolved [48-49]. The signals at binding energies of ~67.7 eV and 67.0 eV can be assigned to Ni^{2+} 3p [50-52] of La_2NiO_{4+d} and $La_2NiO_3F_2$, respectively, which is in agreement with the small reduction of the oxidation state as obtained from titration experiments. In combination with a determination of the anion content from the analysis of the neutron powder diffraction data (see later in this section), it can be concluded that the new compound has an approximate composition of $La_2NiO_3F_2$ (more precisely: $La_2NiO_{3.06}F_{1.94}$). In agreement with previous findings for the syntheses of perovskite and Ruddlesden-Popper type oxyfluorides [53-56], this corresponds to a nearly stoichiometric incorporation of the fluoride ions from the polymer.

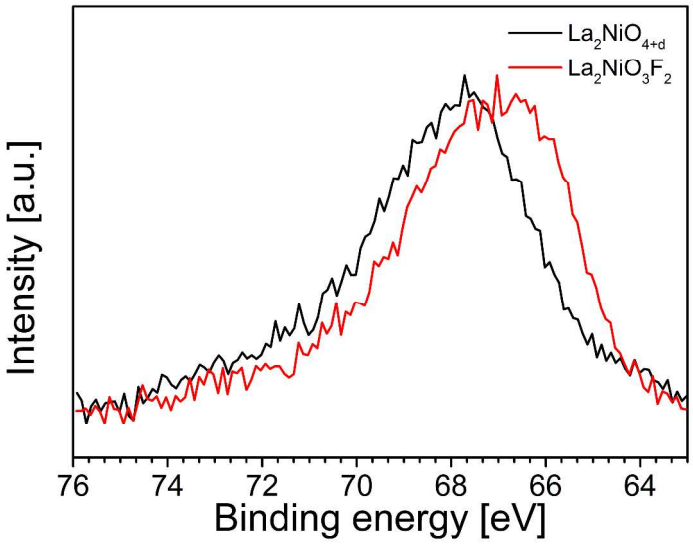

Figure 2: Ni 3p XPS spectrum of La_2NiO_{4+d} and $La_2NiO_3F_2$.

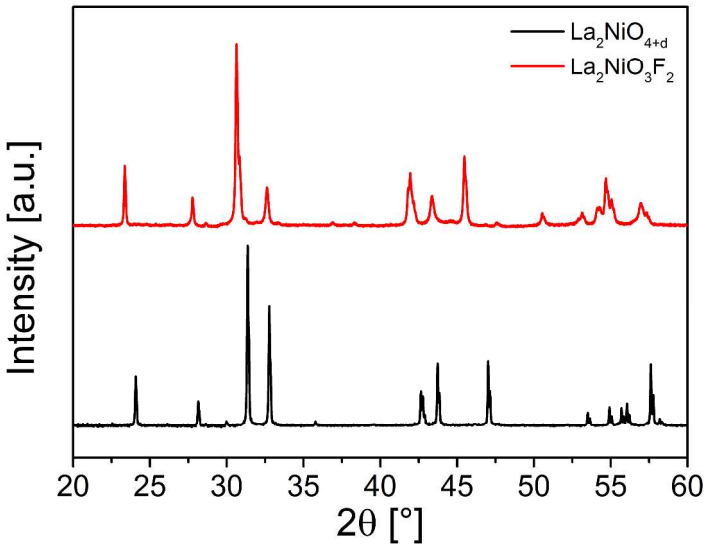

Figure 3: X-ray diffraction patterns of La_2NiO_{4+d} and $La_2NiO_3F_2$.

When comparing the X-ray diffraction patterns of the precursor oxide La_2NiO_{4+d} (d ~ 0.05) to the one of $La_2NiO_3F_2$ (Figure 3), significant changes can be observed. La_2NiO_{4+d} crystallizes in the n=1 Ruddlesden-Popper type structure (a = 3.86279(5) Å and c = 12.6746(2) Å, tetragonal space group *I*4/*mmm* within the resolution of the device used), in good agreement with previous works [57-58]. The pattern of $La_2NiO_3F_2$, on the other hand, showed a clear splitting of some reflections indicating symmetry lowering to orthorhombic.

Fits of the pattern were attempted using a face centered unit cell with a size √2 x √2 x 1 of the parent unit cell with symmetry of *I4/mmm*, which allowed to fit the main reflections. In contrast to what was found previously for the fluorination of K_2NiF_4 type compounds, no strong increase of the c-axis was observed, and the orthorhombic distortion resulted mainly in a strong straining within the *ab* plane, with axis lengths of a ≈ 5.79 Å and b ≈ 5.49 Å. This orthorhombic straining is to the best of our knowledge, one of the highest (if not the highest) straining found for anion excess K_2NiF_4 type compounds A_2BX_{4+y}.

Further loss of translational symmetry was indicated from the presence of superstructure reflections (e.g. (310), (112), (221), (510) with indexes given in relation to the orthorhombic √2 x √2 x 1 cell). These could originate from small distortions or ordering scenarios of anions, which are difficult to determine based on XRD only. Therefore, a coupled Rietveld analysis of XRD and NPD data (Figure 4) was performed. The patterns could be best fitted using a structural model with space group *Cccm (a* = 12.8364(3) Å, b = 5.7940(2) Å and c = 5.4871(2) Å). This tilt system is theoretically possible [59] (a^-a^-0/a^-a^-0 in Glazer's notation, (ϕ ϕ 0)(ϕ ϕ 0) in the notation by Aleksandrov [59]), and was previously observed for the n=3 Ruddlesden-Popper type compound $La_{3.2}Ba_{0.8}Mn_3O_{10}$ [60] (which does not show occupation of anions in the interlayers). The corresponding symmetry tree is shown in Figure 5. Other *klassengleiche* subgroups of *Fmmm* were also examined, but resulted in significantly worse fits due to the systematic absence of certain reflections, which are clearly visible in the neutron diffraction patterns. Exemplarily, Pawley fits within space group no. *64* are provided in the supporting information (since this is a very common distortion found for many K_2NiF_4 compounds [14, 27], see Figure S 1).

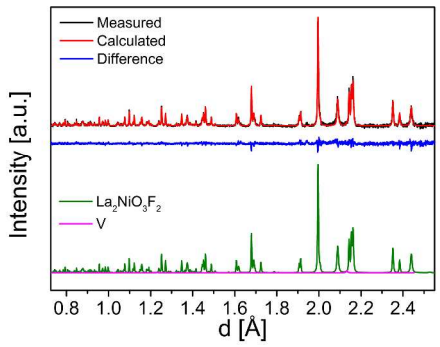

(a)

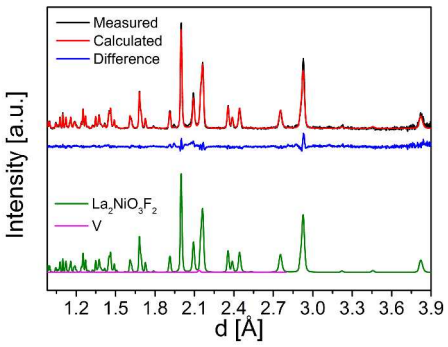

(b)

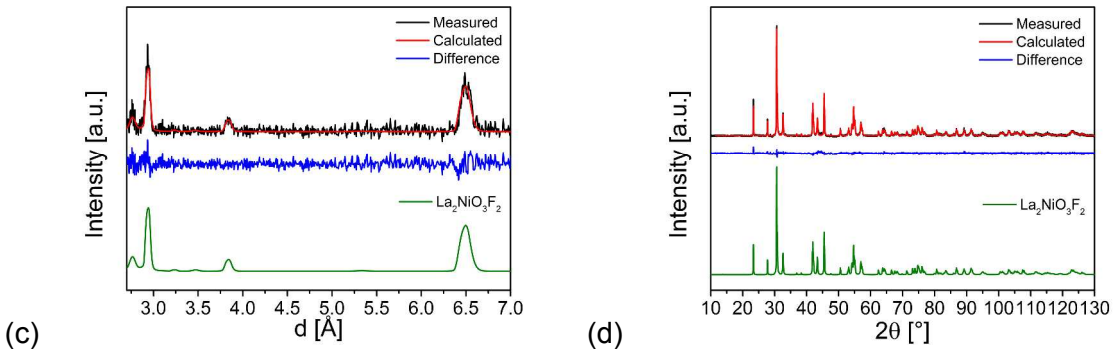

Figure 4: Coupled Rietveld analysis of $La_2NiO_3F_2$ (space group: Cccm) of HRPD bank 1 data (a), HRPD bank 2 data (b), HRPD bank 3 data (c),and XRD data (d).

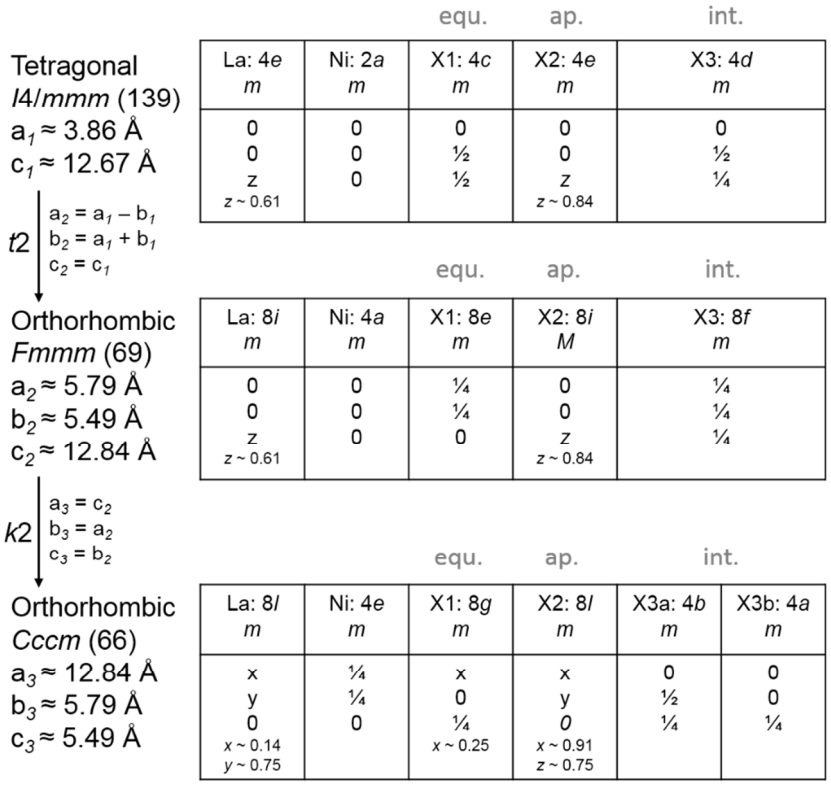

Figure 5: Symmetry tree for the symmetry reduction from I4/mmm to Cccm. Equatorial (equ.), apical (ap.) and interstitial (int.) sites of the anions X are indicated (see also structural data reported in Table 1).

The analysis of the neutron diffraction data facilitates the detailed determination of the structure and composition of the anion sublattice. Here, the reader should be aware that F and O have nearly identical scattering lengths / atomic form factors for neutron and X-ray diffraction, and are indistinguishable with these methods. The analysis of exact bond distances can, however, allow for the assignment of anion sites to one type of anion [13], which will be shown later in this section. Both, the equatorial and apical anion sites, which are fully occupied in the tetragonal starting compound $La_2NiO_{4+d,}$ are fully occupied for the fluorinated material $La_2NiO_3F_2$. The symmetry

reduction from *I*4/*mmm* to *Cccm* results in a splitting of the interlayer anion site into two independent crystallographic sites (Figure 5). The analysis of the neutron diffraction data showed that the 4*a* site is not occupied, whereas the 4b site is fully occupied with one of the anion species. From this, an overall composition of La_2NiX_5 can be derived for the fluorinated compounds, from which, taking into account the presence of single valent Ni^{2+}, the composition $La_2NiO_3F_2$ can be derived. The refined structural parameters are listed in Table 1, a drawing of the refined crystal structure is shown in Figure 6 (with assignment of fluoride and oxide ions to the crystallographic sites as confirmed by bond valence, and NMR analysis, see later in this article). Bond distances are given in Table 2.

In previous reports on oxyfluoride compounds with K_2NiF_4 type structure (e.g. $Sr_2TiO_3F_2$ [21-22] or $LaSrMnO_4F$ [23-24]), a layer wise occupation of every second anion layer was observed, resulting in a symmetry lowering to *P*4/*nmm*. This was found to result in a strong increase of the c-axis from ~ 12.6 Å to ~ 14 Å ($LaSrMnO_4F$) and ~ 15 Å ($Sr_2TiO_3F_2$), without any significant tilting of the MnO_6 or TiO_5F octahedra. This layer wise ordering is symmetry forbidden in *Cccm,* and the site splitting within this space group implies half filling of every interstitial layer in a channel like manner, accompanied by a tilting of the octahedra. This appears to be the origin for the orthorhombic distortion. This ordering scenario does not result in a strong increase of the long crystallographic axis ($c_{I4/mmm}$ resp. a_{Cccm}). Instead, a strong expansion along the $[110]_{I4/mmm}$ direction (along which channels of interstitial anions are formed) and contraction along the $[-110]_{I4/mmm}$ direction were observed (along which the tilting of the octahedra takes place).

Table 1: Structural parameters for $La_2NiO_3F_2$ (space group: Cccm) from coupled Rietveld analysis of XRD and NPD data.

Atom	**Wyckoff site**	**x**	**y**	**z**	**Occ.**	**B [Å^2]**
La1	8l	0.38826(4)	0.7458(2)	**0**	1	1.05(3)
Ni1	4e	¼	¼	**0**	1	1.61(4)
O1@X1 (equ.)	8g	0.2673(2)	**0**	¼	1	1.26(4)
F1@X2 (ap.)	8l	0.5869(2)	0.6576(3)	**0**	1	2.34(6)
O2@X3 (int.)	4b	**0**	½	¼	1	1.26(4)
***a* [Å]**	12.8350(4)	***b* [Å]**	5.7935(2)	***c* [Å]**	5.4864(2)	
R_{wp} **(XRD+NPD) [%]**	3.12	**GOF (XRD+NPD)**	1.58	R_{Bragg} **[%]**	1.13 (XRD) 3.55 (NPD, bank 1)	

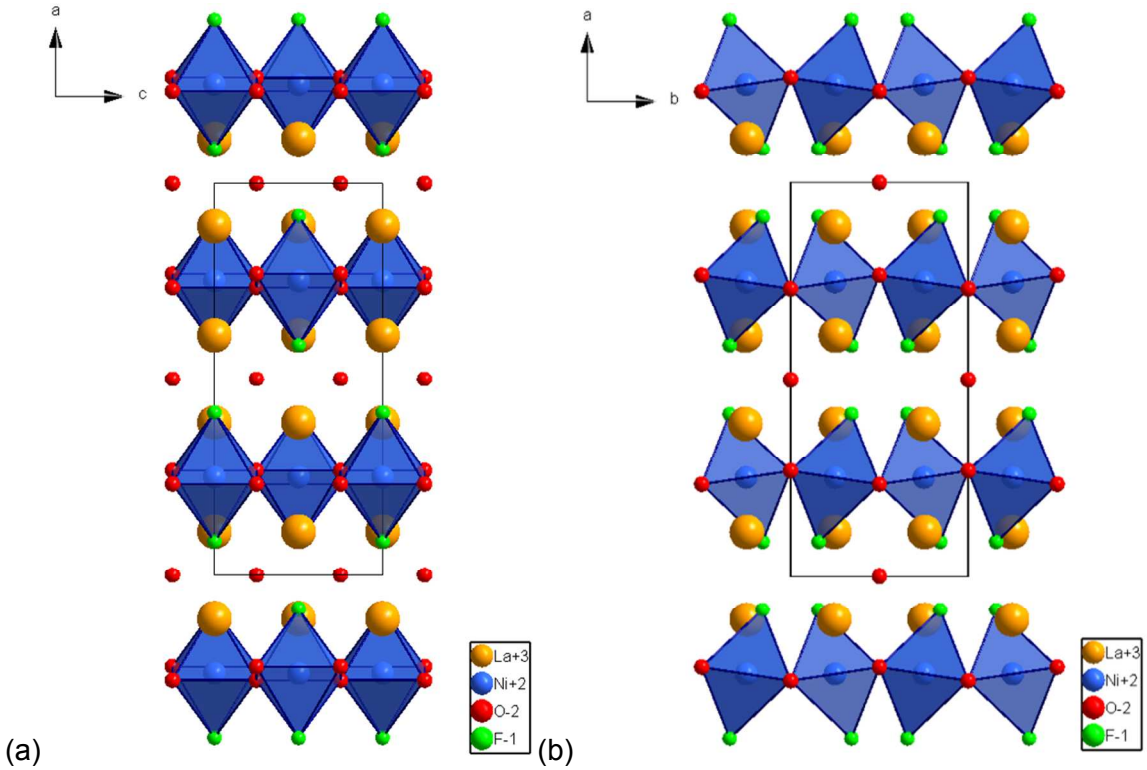

Figure 6: Crystal structure of $La_2NiO_3F_2$ for an $O_{X1} – F_{X2} – O_{X3}$ arrangement on equatorial (X1) and apical (X2) sites of the octahedra as well as in interlayer (X3) sites along different viewing directions (along the b-axis (a) and along the c-axis (b)).

Table 2: Selected bond distances of $La_2NiO_3F_2$ for an $O_{X1} – F_{X2} – O_{X3}$ arrangement on equatorial (X1) and apical (X2) sites of the octahedra as well as in interlayer (X3) sites.

Bond	**Bond distance [Å] in $La_2NiO_3F_2$ with $O_{X1} – F_{X2} – O_{X3}$ distribution**
La1 – X1	2.539(2) [2x]
	2.813(2) [2x]
La1 – X2	2.356(2) [1x]
	2.602(2) [1x]
	2.809(1) [2x]
La1 – X3	2.4718(8) [2x]
Ni1 – X1	2.0076(2) [4x]
Ni1 – X2	2.160(2) [2x]

As discussed above, oxide and fluoride ions are not easily distinguishable, neither by X-ray nor by neutron diffraction. Previously, bond valence sum calculations were shown to be capable [13] to assign oxide and fluoride ions to the respective crystallographic sites. Therefore, different distribution models of oxide and fluoride ions were tested. Table 3 lists results of calculations for

different arrangements on equatorial (X1) and apical sites (X2) of the octahedra as well as on interlayer sites (X3) for the determined composition $La_2NiO_3F_2$ (mixed sites correspond to an occupation of 50 % oxide and 50 % fluoride). The different models can be judged by the so-called global instability index (GII), where a lower index corresponds to a more stable structural arrangement [61]. The highest GIIs were found for anion distributions for which the equatorial anion site (X1) was (partially) replaced by fluoride ions (F1). Thus, these configurations can be excluded, and this agrees well with previous studies on Ruddlesden-Popper type oxyfluorides [13]. For an occupation of the equatorial anion site (X1) by oxide ions, two different distributions of oxide and fluoride ions on the remaining sites (X2 and X3) can be considered: one configuration with an occupation of the interlayers (X3) by oxide ions and occupation of the apical anion site (X2) by fluoride ions, and a second configuration with occupation of the interlayer site (X3) by fluoride ions and mixed occupation of the apical site (X2) by fluoride and oxide ions. The most stable configuration was found for the configuration with the interlayer site (X3) being occupied by oxide ions and the apical site (X2) being occupied by fluoride ions. This result is surprising, since a significant occupation of the interlayer site by oxide ions was never observed before for oxyfluoride compounds with Ruddlesden-Popper type structure.

Table 3: Results of bond valence sum calculations for $La_2NiO_3F_2$ for different O/F distributions on equatorial (X1) and apical (X2) sites of the octahedra as well as in interlayer (X3) sites.

Arrangement of O/F equatorial – apical – interlayers	**Bond valence sum**	**Global Instability Index (GII)**
$O_{X1} – F_{X2} – O_{X3}$	O1: 1.83	0.19
	F2: 1.25	
	O3: 1.67	
$(O/F)_{X1} – (O/F)_{X2} – O_{X3}$	O1: 1.83	0.33
	F1: 1.52	
	O2: 1.54	
	F2: 1.25	
	O3: 1.67	
$F_{X1} – O_{X2} – O_{X3}$	F1: 0.52	0.37
	O2: 1.54	
	O3: 1.67	
$O_{X1} – (O/F)_{X2} – F_{X3}$	O1: 1.84	0.27
	O2: 1.54	
	F2: 1.25	
	F3: 1.33	
$(O/F)_{X1} – O_{X2} – F_{X3}$	O1: 1.83	0.34
	F1: 1.52	
	O2: 1.54	
	F3: 1.33	

^{19}F NMR spectroscopy is a powerful tool to understand the local structure of fluoride ions in a compound. The assignment of the ^{19}F resonance in $La_2NiO_3F_2$ can be assisted by analyzing model systems for which the crystal structure is understood, as for example $Sr_2TiO_3F_2$ [21-22, 28] and its topochemically reduced/hydride-substituted version $Sr_2TiO_3FH_{0.48}$ compound [28]. $Sr_2TiO_3F_2$ is a diamagnetic compound, which structure has been thoroughly characterized with neutron diffraction and EXAFS/XANES spectroscopy. In this compound, the fluoride ions are distributed in a 1:1 ratio on the apical and interstitial anion sites. The ^{19}F MAS NMR spectrum of the compound is shown in Figure 7 a and b. Two groups of signals at approximately -58 and -120 ppm with an intensity ratio of ~ 50:50 can be observed, which is in agreement with the distribution of fluoride ions on the apical and interstitial sites. From the analysis of the spinning sidebands (Figure 7 a), it is apparent that the resonance at -58 ppm has a larger anisotropy. Hence, it should correspond to the apical anion site, which has a more distorted local geometry than the interstitial site.

This assignment of the fluoride ions to the two different sites is further supported by the investigation of $Sr_2TiO_3FH_{0.48}$, obtained from chemical reduction of $Sr_2TiO_3F_2$ with NaH. The reaction causes the substitution of fluoride by hydride in combination with a reductive deintercalation of fluoride only from the interstitial site only and leads to the reduction of ~ 50 % of the Ti^{4+} ([Ar] $3d^0$) to Ti^{3+} ([Ar] $3d^1$) . The remaining fluoride ions in $Sr_2TiO_3FH_{0.48}$ were found to be located only on the apical site, as confirmed by neutron diffraction experiments. Indeed, strong changes were found in the ^{19}F MAS NMR spectrum of $Sr_2TiO_3FH_{0.48}$ (Figure 7 c). The signal of interstitial fluoride (-120 ppm) is absent and two new resonances are observed at -222 ppm and -86 ppm, which match the chemical shift of NaF and SrF_2 [62], both side products of the reduction reaction. The signal from apical fluoride bonded to Ti^{4+} (-58 ppm) is still present, indicating that not all titanium sites were reduced. Nonetheless, a third new resonance at higher chemical shift is present at -38 ppm, a signal that can be attributed to apical fluoride bonded to Ti^{3+}. The unpaired electron in the latter should cause a paramagnetic shift for the fluoride on the apical position, shifting it by $\Delta\delta$=+20 ppm.

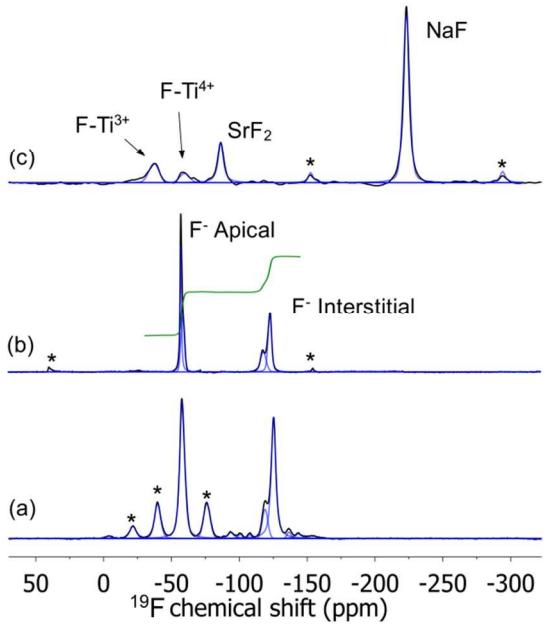

Figure 7. ^{19}F MAS NMR spectra of (a) $Sr_2TiO_3F_2$ (MAS frequency of 10 kHz), (b) $Sr_2TiO_3F_2$ (MAS frequency of 45 kHz), (c) $Sr_2TiO_3FH_{0.48}$ (MAS frequency of 40 kHz). Spinning sidebands marked with an asterisks.

The ^{19}F MAS NMR spectrum of $La_2NiO_3F_2$ (Figure 8 a) shows significantly broader peaks, which result from paramagnetic interactions to the Ni^{2+} ions within the sample. The inhomogeneous contribution of this interaction can be partially averaged by MAS at 55 kHz; nonetheless considerable spinning sidebands are still present in the spectrum. The position of the isotropic peak can be determined by measuring the sample at different MAS frequencies (Figure 8 b) and

a chemical shift of -44 ppm is found for $La_2NiO_3F_2$. Within the limit of resolution, we can assume the presence of a single fluoride site in this compound. From the value of the chemical shift, which is very close to the apical site (-58 to -38 ppm) of the model compounds $SrTiO_3F_2$ / $Sr_2TiO_3FH_{0.48}$, respectively, we conclude that the fluoride ions are located at the apical anion site in $La_2NiO_3F_2$. Due to the strong broadening of the NMR data, a small degree of disordering of fluoride ions cannot be excluded. In this respect, it should be noted that the DFT calculations indicate that off-center shifts should be expected for octahedra with composition NiO_5F (see section 3.4, as also found for $Sr_2TiO_3F_2$ [28]). We therefore also tested a structural model, which allows for off-center shifts of the Ni ion in addition to the occupation of the ideal high symmetry site in the center of the octahedron. The model only resulted in a very small improvement of the fit (as does every model with an increased flexibility), and it was indicated that at least 86 % of the Ni ions are located on the ideal site in the center of the octahedron (Table S 1). Again, this is in agreement with the fluoride ions being only located on the apical anion site (X2), and oxygen being located on the interstitial site (X3).

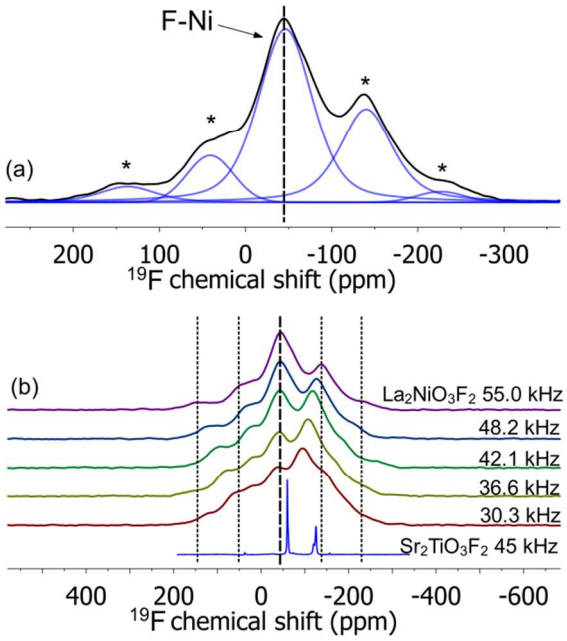

Figure 8: ^{19}F MAS NMR spectra of (a) $La_2NiO_3F_2$ (MAS frequency of 55 kHz), spinning sidebands marked with asterisks, (b) $La_2NiO_3F_2$ (decreasing MAS frequencies from 55 to 30 kHz) and comparison to $Sr_2TiO_3F_2$ (MAS frequency of 45 kHz).

It is very interesting to discuss the structure in the context of other orthorhombic n = 1 Ruddlesden-Popper type compounds A_2BO_4. This can be exemplified by a comparison of the structure of orthorhombic La_2NiO_4 (as determined by Rodriguez-Carvajal et al. [27]) and $La_2NiO_3F_2$ (Figure 9 a). For space group no. 64, the tilting of the octahedra between neighboring layers is in

phase, whereas it is antiphase for space group no. 66. This results in interstitial cavities with identical size for space group no. 64 and in interstitial cavities with different size for space group no. 66 from the symmetry restrictions of both space groups. This size difference for space group no. 66 is well represented by the distance of the apical fluoride ions to the interstitial sites 4a and 4b, which are 1.995(2) Å and 2.654(2) Å approximately. Regarding the sizes of the fluoride and oxide ions of 1.33 Å and 1.40 Å [63], this distortion avoids the formation of very short anion-anion distances, accompanied by the expansion of the b-axis along which the tilting of the octahedra mainly takes place.

We also would like to point out that the ordering scenarios are agreeing well with symmetries around the stage ordering found in superstructures of oxidized La_2NiO_{4+d} [64] or La_2CuO_{4+d} [65] (Figure 9 b). For such stage ordering, the layers with intercalated ions form a twinning plane, and only the large interstitial sites are reported to be occupied with oxide ions [64]. Therefore, the structure of $La_2NiO_3F_2$ with space group *Cccm* can also be understood as the stage structure of the n = 1 orthorhombic (*Bbcm*) Ruddlesden-Popper type structure with stage 1 ordering.

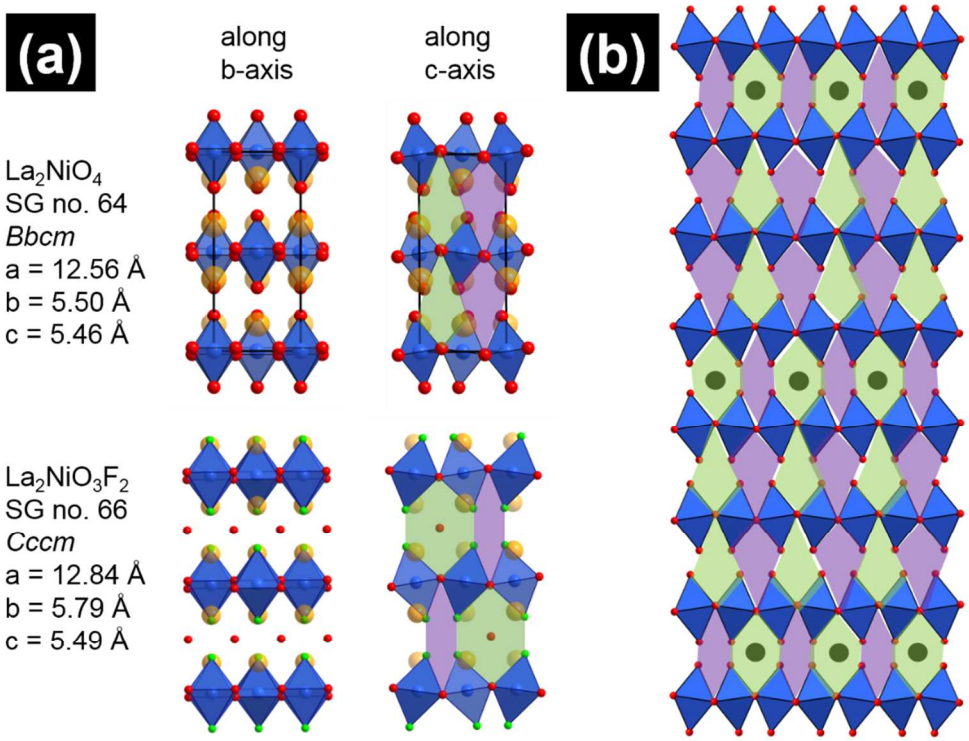

Figure 9: (a) Comparison of the structure of orthorhombic La_2NiO_4 (SG no. 64 (given in the non-conventional setting for easier comparability), data from ref. [27]) and $La_2NiO_3F_2$ (SG no. 66). (b) Stage 3 ordering of interstitial oxide ions of oxidized La_2NiO_{4+d} as proposed in ref. [64].

3.2 High-temperature X-ray Diffraction Study

In order to investigate the decomposition behavior and the temperature stability of $La_2NiO_3F_2$, a high-temperature X-ray diffraction study was performed (Figure 10 a and b). With increasing temperature, reflections shift towards lower diffraction angles due to thermal lattice expansion. Apart from the presence of a very small amount of LaF_3, LaOF is formed as a decomposition product at 500 °C, which is a well-known behavior found for heating of oxyfluoride materials [66]. At temperatures above 500 °C, only LaOF can be found, indicating that amorphization of the Ni-containing fraction is taking place.

From the shifts of different reflections on heating (Figure 10 b), reflected in the trend of the determined lattice parameters (Figure 10 c), it becomes apparent that the thermal expansion is anisotropic. While the increase of each of the three lattice parameters is fairly linear with temperature (the lattice parameters obtained at 500 °C have to be excluded due to the onset of decomposition), a and c show a significantly stronger increase than b. Thus, the orthorhombic distortion decreases on heating of the compound. However, a complete transition towards the tetragonal crystal system cannot be achieved prior to decomposition, indicating that the ordering of the oxide ions on the interstitial sites shows a high thermal stability. From this, we conclude that there is no indication for strong disordering of oxide ions due to entropic effects on the interstitial sites on increasing of the temperature below the decomposition point.

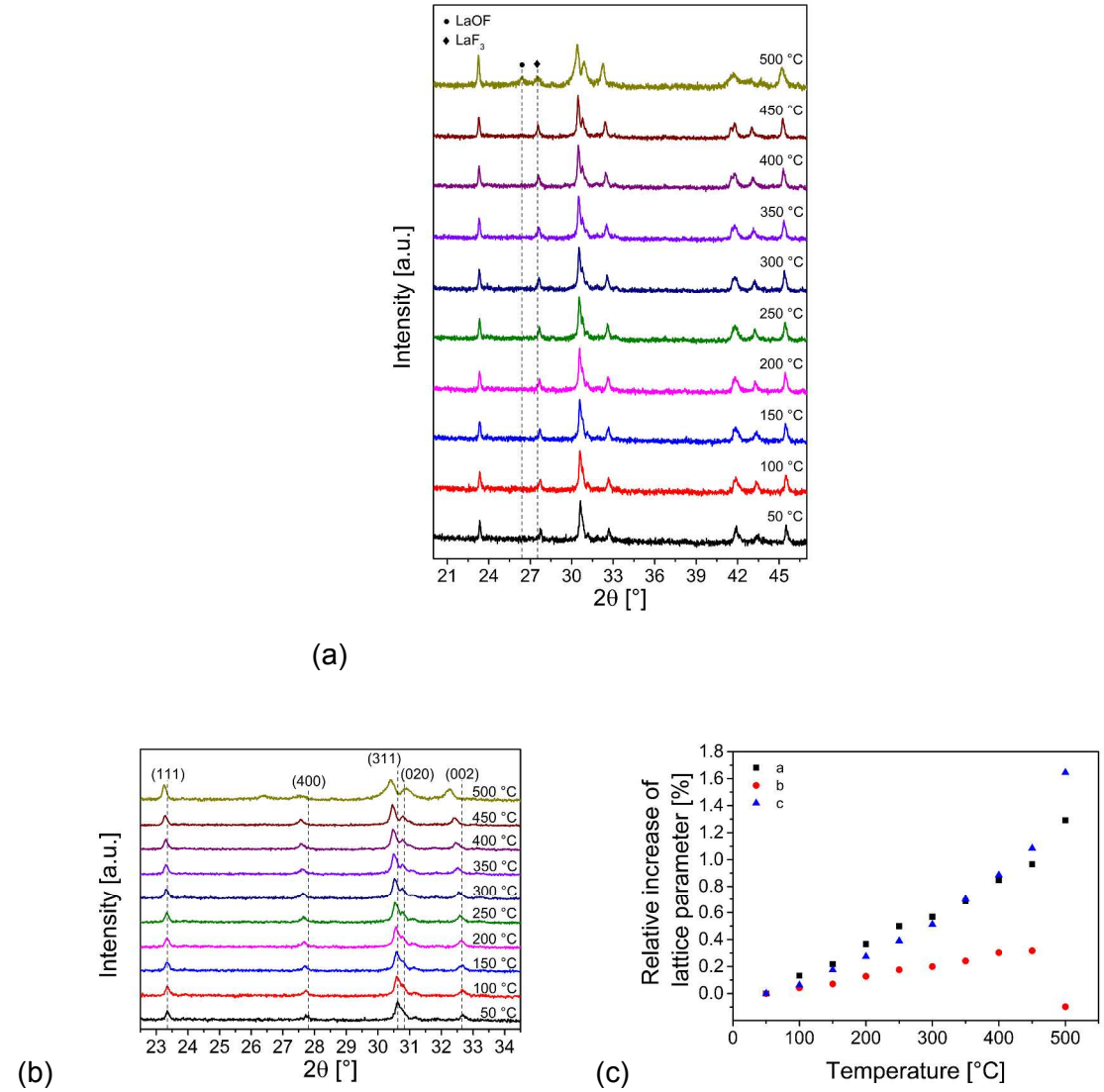

Figure 10: (a) High-temperature X-ray diffraction patterns of $La_2NiO_3F_2$ in a temperature range from 50 °C to 500 °; impurity phase and decomposition products are marked with • and ♦ for LaOF and LaF_3, respectively). (b) High-temperature X-ray diffraction patterns with hkl indices for the strongest reflections of the $La_2NiO_3F_2$ phase in the 2Θ range between 22.5° and 34.5° (positions of hkl indicators are set to their respective positions at 50 °C). (c) Relative increase of the lattice parameters as a function of temperature.

3.3 Magnetic Characterization

The variation of magnetic magnetization (black curve) of $La_2NiO_3F_2$ upon temperature increase from 5 K to 350 K following cooling in zero applied field (ZFC) and applied field (FC) of μ_0H = 1 T are given in Figure 11 a. No deviations between the ZFC and FC measurement were observed. Above 49 K, a paramagnetic behavior is observed. Between 150 K and 300 K, inverse susceptibility data (red curve) are linear and can be fitted in accordance with the Curie-Weiss

law. The obtained paramagnetic moment of 2.82 μ_B agrees well with the expected spin-only magnetic moment of high-spin Ni^{2+} (2.83 μ_B). A Weiss constant of $\Theta \approx -648$ K indicates that strong anitferromagnetic interactions are taking place. The presence of high-spin Ni^{2+} is in agreement with the comparably small distortion of the octahedron.

At 49 K, a transition from paramagnetic towards antiferromagnetic behavior was observed. The increase of the magnetization at temperatures below 30 K suggests the contribution of a weak ferromagnetic component, which could originate from a magnetic canting within the compound on antiferromagnetic ordering [27].

To confirm the origin of ferromagnetism below 30 K, we carried out field-dependent measurements at 5 K. The magnetic field was scanned from 3 T to -3 T and the magnetization was measured, as given in Figure 11 b. The observed weak hysteresis confirms an intrinsic ferromagnetic component. In addition, we observe an exchange-bias (E_B) with an E_B field of -0.17 T. The presence of such an exchange anisotropy can be explained by co-existence of ferromagnetic and antiferromagnetic components in the system. The predominant hard antiferromagnetic component pins the soft ferromagnetic component showing a shift in the hysteresis from origin. This shift is, however, seen to significantly reduce when measured at 49K, due to a strong antiferromagnetic coupling at the Néel temperature and temperature dependent decay of the ferromagnetic component. Furthermore, a similar FC and ZFC temperature dependent magnetization rules out the possibility of exchange-bias via spin-glass.

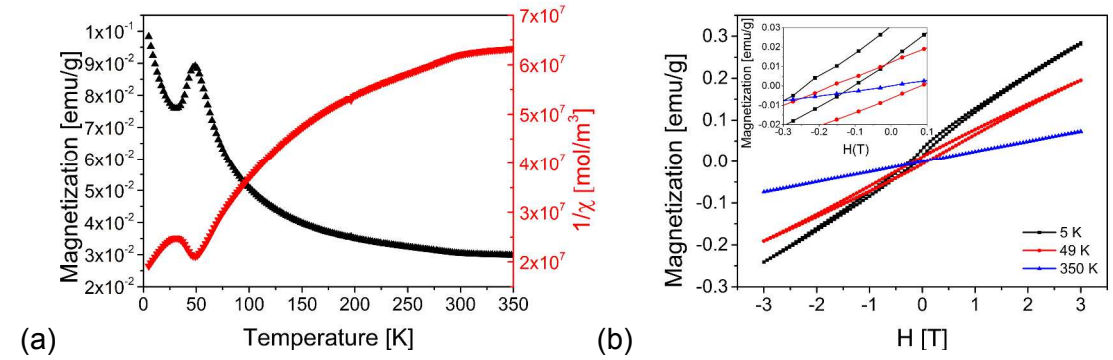

Figure 11: (a) Magnetization vs. temperature curve of $La_2NiO_3F_2$ measured at μ_0H = 1 T (black, FC and ZFC curves overlap), and inverse susceptibility vs. temperature curve of $La_2NiO_3F_2$ (red), (b) Magnetization vs. magnetic field curve of $La_2NiO_3F_2$ measured at 5 K, 49 K and 350 K; the inset shows the exchange bias observed at 5 K.

A comparison between the magnetic behaviors of $La_2NiO_3F_2$ and the parent compound La_2NiO_{4+d} is interesting at this point. Stoichiometric La_2NiO_4 orders anitferromagnetically below 330 K, and the magnetic structure can be described in the magnetic space group *Pccn* with G-

type ordering of magnetic moments within the *bc* plane (respectively within the tetragonal ab plane) [27]. Such alignment of magnetic moments within the *bc* plane is also possible within two of the maximum magnetic space groups of *Cccm* with k = [0 0 0], being *Cccm* (66.491, AFM along z) and *Ccc'm'* (66.496, AFM along y). Both models were tried and resulted in magnetic moments of Ni below 0.1 μ_B, which is not significant, and therefore in agreement with the paramagnetic nature at room temperature. Other magnetic ordering scenarios with k ≠ [0 0 0] at ambient temperature can be ruled out from the absence of additional reflections in the pattern. The superexchange via the apical fluoride ions appears to weaken the Ni-F-F-Ni superexchange interactions, which are responsible for establishing magnetic ordering between the layers.

3.4 DFT+U Calculations

In our previous studies [14-15, 28], we have shown that DFT calculations can also help to elucidate the structure of the anion sublattice, and to provide understanding for stabilities of different anion ordering scenarios. Therefore, different ordering scenarios were tested for $La_2NiO_3F_2$. Interestingly, the experimentally determined anion distribution $O_{X1} – F_{X2} – O_{X3}$ was not found to be energetically most favorable. The configurations of $O_{X1} – (O/F)_{X2} – O_{X3}$ v1 and v2 were found to show lower energies per $La_2NiO_3F_2$ formula unit (Δ = -0.06 – 0.04 eV), and a strong structural distortion to monoclinic symmetry. However, these energy differences are small (and "0 K energies"), being in the same order of magnitude than the thermal energy at synthesis temperature (~ 0.05 eV). Remarkably, bond valence sums calculations were able to predict the ordering of oxide and fluoride ions verified via the ^{19}F NMR studies correctly, which can be understood from the fact that they originate from the evaluation of experimentally obtained bond distances.

The structural distortions found for the structures after DFT optimization strongly differ for the different anion configurations. In this respect, we would like to emphasize that the $O_{X1} – F_{X2} – O_{X3}$ configuration is the one with lowest energy while maintaining the highest possible orthorhombic symmetry (i.e., without transforming to monoclinic). This orthorhombic symmetry was only obtained for the $O_{X1} – (O/F)_{X2} – F_{X3}$ v3 configuration, which has a considerably higher energy than the $O_{X1} – F_{X2} – O_{X3}$ configuration (Δ = +0.18 eV per $La_2NiO_3F_2$ formula unit, corresponding to ~3.5 times of the thermal energy at synthesis temperature). Combining both, consideration of the calculated structural distortions and energy, we conclude that the experimentally observed structure might be understood as the best compromise between energy and symmetry.

Further, we note that the models O_{X1} – $(O/F)_{X2}$ – F_{X3} v1, v2 and v3 show strong off-centre shift of the Ni ion within the octahedral of composition NiO_5F towards the apical oxide ion. Again, this can be ruled out from the refinement of XRD and NPD data with a structural model, which allows for off-centre displacement of the Ni cations (see section 3.1).

Table 4: Energies obtained from DFT calculations for $La_2NiO_3F_2$ for different O/F distributions on equatorial (X1), apical (X2), and interlayer (X3) sites.

Arrangement of O/F equatorial – apical – interlayers	**Energy difference per $La_2NiO_3F_2$ formula unit [eV] to the O_{X1} – F_{X2} – O_{X3} configuration**
O_{X1} – F_{X2} – O_{X3}	0
O_{X1} – $(O/F)_{X2}$ – F_{X3} v1	-0.06
O_{X1} – $(O/F)_{X2}$ – F_{X3} v2	-0.04
O_{X1} – $(O/F)_{X2}$ – F_{X3} v3	+0.18
O_{X1} – $(O/F)_{X2}$ – F_{X3} v4	+0.22

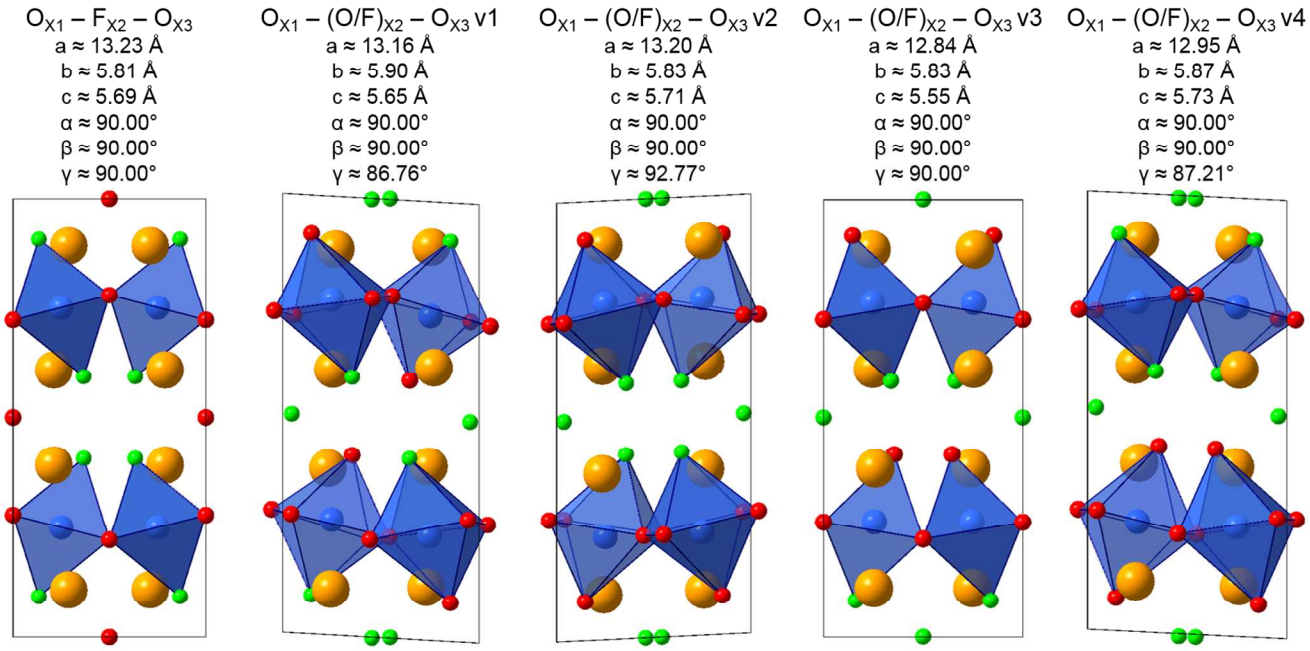

Figure 12: Optimized structures of $La_2NiO_3F_2$ calculated from DFT for different O/F distributions on equatorial (X1), apical (X2), and interlayer (X3) sites with corresponding lattice parameters. Unit cells are depicted along the c-axis.

4 Conclusions

Here, we have demonstrated that $La_2NiO_3F_2$ shows an unusual ordering of anions in the interlayer. Whereas oxyfluoride compounds with Ruddlesden-Popper were previously found to

show a strong expansion of the lattice along the stacking direction of the perovskite layers, a channel like ordering of oxide ions on the interlayer sites results in an expansion of the lattice perpendicular to the stacking direction, accompanied by a strong tilting of the NiO_4F_2 octahedra. Furthermore, the compound is so far the only known oxyfluoride with Ruddlesden-Popper type structure, which shows preferred occupation of the interlayer sites by oxide instead of fluoride ions. The fluorination results in a strong decrease of the magnetic ordering temperature, which most likely arises from a weakening of the Ni-F-F-Ni superexchange interactions between the perovskite type layers due to a reduced covalency of the fluoride ion.

Clearly, low temperature neutron diffraction studies will be required to understand the low temperature magnetic properties and structure of the compound in more detail. Here, it would be interesting to see if the ferromagnetic moment below 30 K could originate from a magnetic canting within an antiferromagnetic arrangement, which would be symmetry allowed for some of the magnetic subgroups of *Cccm*.

5 Acknowledgements

This work was funded by the German Research Foundation within the Emmy Noether program (Grant No. CL551/2-1). Neutron diffraction beam time on HRPD at ISIS was provided by the Science and Technology Facilities Council (STFC) (No. 1720040). Computational time was made available at the Lichtenberg-Cluster at TU Darmstadt, Germany.

6 Supporting Information

The Supporting Information is available free of charge on the ACS Publications website at DOI: .

Pawley fits of HRPD bank 1 data of $La_2NiO_3F_2$ to exclude structural models with space group no. 64, and structural parameters for the Ni ion when using a split side model for the coupled Rietveld analysis of neutron and X-ray diffraction data.

7 References

1. Abakumov, A. M.; Hadermann, J.; Van Tendeloo, G.; Shpanchenko, R. V.; Oleinikov, P. N.; Antipov, E. V., Anion Ordering in Fluorinated La_2CuO_4. *J. Solid State Chem.* **1999,** *142* (2), 440-450.

2. Chevalier, B.; Tressaud, A.; Lepine, B.; Amine, K.; Dance, J. M.; Lozano, L.; Hickey, E.; Etourneau, J., Stabilization of a new superconducting phase by low temperature fluorination of La_2CuO_4. *Phys. C (Amsterdam, Neth.)* **1990,** *167* (1–2), 97-101.

3. Delville, M. H.; Barbut, D.; Wattiaux, A.; Bassat, J. M.; Menetrier, M.; Labrugere, C.; Grenier, J. C.; Etourneau, J., Electrochemical fluorination of La_2CuO_4: a mild "chimie douce" route to superconducting oxyfluoride materials. *Inorg. Chem.* **2009,** *48* (16), 7962-9.

4. Al-Mamouri, M.; Edwards, P. P.; Greaves, C.; Slaski, M., Synthesis and superconducting properties of the strontium copper oxy-fluoride $Sr_2CuO_2F_{2+d}$. *Nature (London, U.K.)* **1994,** *369* (6479), 382-384.

5. Ar-nikova, E. I.; Lubarsky, S. V.; Denisenko, D. I.; Shpanchenko, R. V.; Antipov, E. V.; Van Tendeloo, G., A new way of synthesis and characterization of superconducting oxyfluoride $Sr_2Cu(O, F)_{4+\delta}$. *Phys. C (Amsterdam, Neth.)* **1995,** *253* (3–4), 259-265.

6. Orera, A.; Slater, P. R., New Chemical Systems for Solid Oxide Fuel Cells. *Chem. Mater.* **2010,** *22* (3), 675-690.

7. Zhang, R.; Senn, M. S.; Hayward, M. A., Directed Lifting of Inversion Symmetry in Ruddlesden–Popper Oxide–Fluorides: Toward Ferroelectric and Multiferroic Behavior. *Chem. Mater.* **2016**.

8. Batlett, X.; Obradors, X.; Sayagués, M. J.; Vallet, M.; González-Calbet, J. M., Weak ferromagnetism and magnetic interactions in La_2NiO_4. *J. Phys.: Condens. Matter* **1992,** *4*, 487-496.

9. Zhang, R.; Read, G.; Lang, F.; Lancaster, T.; Blundell, S. J.; Hayward, M. A., $La_2SrCr_2O_7F_2$: A Ruddlesden-Popper Oxyfluoride Containing Octahedrally Coordinated Cr(4+) Centers. *Inorg. Chem.* **2016,** *55* (6), 3169-74.

10. Kendall, K. R.; Navas, C.; Thomas, J. K.; zur Loye, H.-C., Recent Developments in Oxide Ion Conductors: Aurivilius Phases. *Chem. Mater.* **1996,** *8* (3), 642-649.

11. Greaves, C.; Francesconi, M. G., Fluorine insertion in inorganic materials. *Curr. Opin. Solid State Mater. Sci.* **1998,** *3* (2), 132-136.

12. McCabe, E. E.; Greaves, C., Review: Fluorine insertion reactions into pre-formed metal oxides. *J. Fluorine Chem.* **2007,** *128*, 448-458.

13. Clemens, O.; Slater, P. R., Topochemical modifications of mixed metal oxide compounds by low-temperature fluorination routes. *Reviews in Inorganic Chemistry* **2013,** *33* (2-3), 105-117.

14. Nowroozi, M. A.; Ivlev, S.; Rohrer, J.; Clemens, O., La_2CoO_4: a new intercalation based cathode material for fluoride ion batteries with improved cycling stability. *J. Mater. Chem. A* **2018,** *6* (11), 4658-4669.

15. Nowroozi, M. A.; Wissel, K.; Rohrer, J.; Munnangi, A. R.; Clemens, O., $LaSrMnO_4$: Reversible Electrochemical Intercalation of Fluoride Ions in the Context of Fluoride Ion Batteries. *Chem. Mater.* **2017**.

16. Kissick, J. L.; Greaves, C.; Edwards, P. P.; Cherkashenko, V. M.; Kurmaev, E. Z.; Bartkowski, S.; Neumann, M., Synthesis, structure, and XPS characterization of the stoichiometric phase $Sr_2CuO_2F_2$. *Phys. Rev. B.* **1997,** *56* (5), 2831-2835.

17. D'Arco, S.; Islam, M. S., Defect and dopant properties of the oxyfluoride superconductor $Sr_2CuO_2F_{2+\delta}$. *Phys. Rev. B: Condens. Matter Mater. Phys.* **1997,** *55* (5), 3141-3145.

18. Heap, R. S., P.R., Synthesis of $Ca_{2-x}Sr_xCuO_2F_2$ (0 ≤x≤ 2) with the T'-structure through fluorination of $Ca_{2-x}Sr_xCuO_3$with poly(vinylidenefluoride)/poly(tetrafluoroethylene). University of Birmingham Chemistry Paper ID code 1667 Avialable at: http://epapers.bham.ac.uk/1667/, 2009.

19. Baikie, T.; Young, N. A.; Francesconi, M. G., Synthesis and low temperature fluorination of the alkaline-earth palladates $Ba_{2-x}Sr_xPdO_3$ (x=0–2). *Prog. Solid State Chem.* **2007,** *35* (2), 265-279.

20. Al-Mamouri, M.; Edwards, P. P.; Greaves, C.; Slater, P. R.; Slaski, M., Synthesis and structure of the calcium copper oxyfluoride, $Ca_2CuO_2F_{2+d}$. *J. Mater. Chem.* **1995,** *5* (6), 913-916.

21. Slater, P. R.; Gover, R. K. B., Synthesis and structure of the new oxide fluoride $Sr_2TiO_3F_2$ from the low temperature fluorination of Sr_2TiO_4: an example of a staged fluorine substitution/insertion reaction. *J. Mater. Chem.* **2002,** *12* (2), 291-294.

22. Slater, P. R., Poly(vinylidene fluoride) as a reagent for the synthesis of K_2NiF_4-related inorganic oxide fluorides *J. Fluorine Chem.* **2002,** *117*, 43-45.

23. Aikens, L. D.; Li, R. K.; Greaves, C., The synthesis and structure of a new oxide fluoride, $LaSrMnO_4F$, with staged fluorine insertion. *Chem. Commun.* **2000,** (21), 2129-2130.

24. Aikens, L. D.; Gillie, L. J.; Li, R. K.; Greaves, C., Staged fluorine insertion into manganese oxides with Ruddlesden–Popper structures: $LaSrMnO_4F$ and $La_{1.2}Sr_{1.8}Mn_2O_7F$. *J. Mater. Chem.* **2002,** *12* (2), 264-267.

25. Slater, P. R.; Gover, R. K. B., Synthesis and structure of the new oxide fluoride $Ba_2ZrO_3F_2$ * x H_2O (x ~ 0.5). *J. Mater. Chem.* **2001,** *11* (8), 2035-2038.

26. Hancock, C. A.; Herranz, T.; Marco, J. F.; Berry, F. J.; Slater, P. R., Low temperature fluorination of $Sr_3Fe_2O_{7-x}$ with polyvinylidine fluoride: An X-ray powder diffraction and Mössbauer spectroscopy study. *J. Solid State Chem.* **2012,** *186*, 195-203.

27. Rodriguez-Carvajal, J.; Fernandez-Diaz, M. T.; Martinez, J. L., Neutron diffraction study on structural and magnetic properties of La_2NiO_4. *J. Phys.: Condens. Matter* **1991,** *3*, 3215-3234.

28. Wissel, K.; Dasgupta, S.; Benes, A.; Schoch, R.; Bauer, M.; Witte, R.; Fortes, A. D.; Rohrer, J.; Clemens, O., Developing intercalation based anode materials for fluoride-ion batteries: Topochemical reduction of $Sr_2TiO_3F_2$ via a hydride based defluorination process. *J. Mater. Chem. A* **submitted**.

29. Ibberson, R. M., Design and performance of the new supermirror guide on HRPD at ISIS. *Nuclear Instruments and Methods in Physics Research Section A: Accelerators, Spectrometers, Detectors and Associated Equipment* **2009,** *600* (1), 47-49.

30. Ibberson, R. M. D., W.I.F.; Knight, K.S., The high resolution powder diffractometer (HRPD) at ISIS - a user guide. **1992**.

31. Arnold, O.; Bilheux, J. C.; Borreguero, J. M.; Buts, A.; Campbell, S. I.; Chapon, L.; Doucet, M.; Draper, N.; Ferraz Leal, R.; Gigg, M. A.; Lynch, V. E.; Markvardsen, A.; Mikkelson, D. J.; Mikkelson, R. L.; Miller, R.; Palmen, K.; Parker, P.; Passos, G.; Perring, T. G.; Peterson, P. F.; Ren, S.; Reuter, M. A.; Savici, A. T.; Taylor, J. W.; Taylor, R. J.; Tolchenov, R.; Zhou, W.; Zikovsky, J., Mantid—Data analysis and visualization package for neutron scattering and μ SR experiments. *Nuclear Instruments and Methods in Physics Research Section A: Accelerators, Spectrometers, Detectors and Associated Equipment* **2014,** *764* (Supplement C), 156-166.

32. *Topas V5, General profile and structure analysis software for powder diffraction data, User's Manual*. Bruker AXS: Karlsruhe, Germany, 2014.

33. Coelho, A. A. TOPAS-Academic. http://www.topas-academic.net (accessed 20th of October 2014).

34. Cheary, R. W., Coelho, A. A., Cline, J. P., Fundamental Parameters Line Profile Fitting in Laboratory Diffractometers. *J. Res. Natl. Inst. Stand. Technol.* **2004,** *109*, 1-25.

35. Shirley, D. A., High-Resolution X-Ray Photoemission Spectrum of the Valence Bands of Gold. *Phys. Rev. B.* **1972,** *5* (12), 4709-4714.

36. Berry, G. A. B. a. J. F., Diamagnetic Corrections and Pascal's Constants. *J. Chem. Educ.* **2008,** *85* (4).

37. de Laune, B. P.; Rees, G. J.; Marco, J. F.; Hah, H.-Y.; Johnson, C. E.; Johnson, J. A.; Berry, F. J.; Hanna, J. V.; Greaves, C., Topotactic Fluorine Insertion into the Channels of $FeSb_2O_4$-Related Materials. *Inorg. Chem.* **2017,** *56* (16), 10078-10089.

38. Blöchl, P. E., Projector augmented-wave method. *Phys. Rev. B.* **1994,** *50* (24), 17953-17979.

39. Kresse, G.; Furthmüller, J., Efficiency of ab-initio total energy calculations for metals and semiconductors using a plane-wave basis set. *Comput. Mat. Sci.* **1996,** *6*, 15.

40. Perdew, J. P.; Burke, K.; Ernzerhof, M., Erratum: Generalized Gradient Approximation Made Simple. *Phys. Rev. Lett.* **1997,** *78*, 1396.

41. Perdew, J. P.; Burke, K.; Ernzerhof, M., Generalized Gradient Approximation Made Simple. *Phys. Rev. Lett.* **1996,** *77*, 3865.

42. Shick, A. B.; Liechtenstein, A. I.; Pickett, W. E., Implementation of the LDA+U method using the full-potential linearized augmented plane-wave basis. *Phys. Rev. B.* **1999,** *60* (15), 10763.

43. Liechtenstein, A. I.; Anisimov, V. I.; Zaanen, J., Density-functional theory and strong interactions: Orbital ordering in Mott-Hubbard insulators. *Phys. Rev. B.* **1995,** *52* (8), R5467.

44. Zhou, F.; Cococcioni, M.; Marianetti, C. A.; Morgan, D.; Ceder, G., First-principles prediction of redox potentials in transition-metal compounds with LDA+U. *Phys. Rev. B.* **2004,** *70* (23), 235121.

45. Wang, L.; Maxisch, T.; Ceder, G., Oxidation energies of transition metal oxides within the GGA+U framework. *Phys. Rev. B.* **2006,** *73*, 195107.

46. Berry, F. J.; Ren, X.; Heap, R.; Slater, P.; Thomas, M. F., Fluorination of perovskite-related $SrFeO_{3-\delta}$. *Solid State Commun.* **2005,** *134* (9), 621-624.

47. Berry, F. J.; Heap, R.; Ö, H.; Moore, E. A.; Shim, S.; Slater, P. R.; Thomas, M. F., Magnetic order in perovskite-related $SrFeO_2F$. *J. Phys.: Condens. Matter* **2008,** *20* (21), 215207.

48. Clauberg, R.; Gudat, W.; Kisker, E.; Kuhlmann, E.; Rothberg, G. M., Nature of the Resonant 6-eV Satellite in Ni: Photoelectron Spin-Polarization Analysis. *Phys. Rev. Lett.* **1981,** *47* (18), 1314-1317.

49. Moulder, J. F.; Chastain, J., *Handbook of X-ray Photoelectron Spectroscopy: A Reference Book of Standard Spectra for Identification and Interpretation of XPS Data*. Physical Electronics Division, Perkin-Elmer Corporation: 1992.

50. Ning, X.; Wang, Z.; Zhang, Z., Fermi level shifting, charge transfer and induced magnetic coupling at $La_{0.7}Ca_{0.3}MnO_3/LaNiO_3$ interface. *Sci Rep* **2015,** *5*, 8460.

51. Liang, Q.; Xiaofang, B., Direct observation of Ni^{3+} and Ni^{2+} in correlated $LaNiO_{3-\delta}$ films. *EPL (Europhysics Letters)* **2011,** *93* (5), 57002.

52. Marco, J. F.; Gancedo, J. R.; Ortiz, J.; Gautier, J. L., Characterization of the spinel-related oxides $Ni_xCo_{3-x}O_4$ (x=0.3,1.3,1.8) prepared by spray pyrolysis at 350 °C. *Appl. Surf. Sci.* **2004,** *227* (1), 175-186.

53. Clemens, O.; Haberkorn, R.; Slater, P. R.; Beck, H. P., Synthesis and characterisation of the $Sr_xBa_{1-x}FeO_{3-y}$-system and the fluorinated phases $Sr_xBa_{1-x}FeO_2F$. *Solid State Sci.* **2010,** *12* (8), 1455-1463.

54. Clemens, O.; Berry, F. J.; Wright, A. J.; Knight, K. S.; Perez-Mato, J. M.; Igartua, J. M.; Slater, P. R., A neutron diffraction study and mode analysis of compounds of the system $La_{1-x}Sr_xFeO_{3-x}F_x$ (x=1, 0.8, 0.5, 0.2) and an investigation of their magnetic properties. *J. Solid State Chem.* **2013,** *206*, 158-169.

55. Clemens, O.; Kruk, R.; Patterson, E. A.; Loho, C.; Reitz, C.; Wright, A. J.; Knight, K. S.; Hahn, H.; Slater, P. R., Introducing a large polar tetragonal distortion into Ba-doped $BiFeO_3$ by low-temperature fluorination. *Inorg. Chem.* **2014,** *53* (23), 12572-83.

56. Clemens, O., Structural characterization of a new vacancy ordered perovskite modification found for $Ba_3Fe_3O_7F$ ($BaFeO_{2.333}F_{0.333}$): Towards understanding of vacancy ordering for different perovskite-type ferrites. *J. Solid State Chem.* **2015,** *225*, 261-270.

57. Jorgensen, J. D.; Dabrowski, B.; Pei, S.; Richards, D. R.; Hinks, D. G., Structure of the interstitial oxygen defect in $La_2NiO_{4+\delta}$. *Physical Review B* **1989,** *40* (4), 2187-2199.

58. Mehta, A.; Heaney, P. J., Structure of $La_2NiO_{4.18}$. *Physical Review B* **1994,** *49* (1), 563-571.

59. Aleksandrov, K. S.; Bartolomé, J., Structural distortions in families of perovskite-like crystals. *Phase Transitions* **2001,** *74* (3), 255-335.

60. Hadermann, J.; Abakumov, A. M.; Tsirlin, A. A.; Rozova, M. G.; Sarakinou, E.; Antipov, E. V., Expanding the Ruddlesden-Popper manganite family: the N = 3 $La_{3.2}Ba_{0.8}Mn_3O_{10}$ member. *Inorg. Chem.* **2012,** *51* (21), 11487-92.

61. Brown, I. D., The Bond-Valence Method: An Empirical Approach to Chemical Structure and Bonding. In *Industrial Chemistry Library*, O'Keeffe, M.; Navrotsky, A., Eds. Elsevier: 1981; Vol. 2, pp 1-30.

62. Kreinbrink, A. T.; Sazavsky, C. D.; Pyrz, J. W.; Nelson, D. G. A.; Honkonen, R. S., Fast-magic-angle-spinning ^{19}F NMR of inorganic fluorides and fluoridated apatitic surfaces. *J. Magn. Reson.* **1990,** *88* (2), 267-276.

63. Shannon, R. D., Revised Effective Ionic Radii and Systematic Studies of Interatomie Distances in Halides and Chaleogenides. *Acta Crystallographica, Section A: Foundations of Crystallography* **1976,** *A32*, 751-767.

64. Tranquada, J. M.; Kong, Y.; Lorenzo, J. E.; Buttrey, D. J.; Rice, D. E.; Sachan, V., Oxygen intercalation, stage ordering, and phase separation in$La_2NiO_{4+\delta}$ with $0.05 \lesssim \delta \lesssim 0.11$. *Phys. Rev. B.* **1994,** *50* (9), 6340-6351.

65. Rial, C.; Arroyo, E.; Moran, E.; Alario-Franco, M. Á.; Amador, U.; Ehrenberg, H.; Fuess, H., Synchrotron X-ray diffraction study of the phase separation on heating oxidized $La_2CuO_{4.103(4)}$: the stabilization of phase $La_2CuO_{4.086(4)}$. *Physica C* **1999,** *319*, 21-33.

66. Clemens, O.; Kuhn, M.; Haberkorn, R., Synthesis and characterization of the $La_{1-x}Sr_xFeO_{3-delta}$ system and the fluorinated phases $La_{1-x}Sr_xFeO_{3-x}F_x$. *J. Solid State Chem.* **2011,** *184* (11), 2870-2876.

For Table of Contents Only

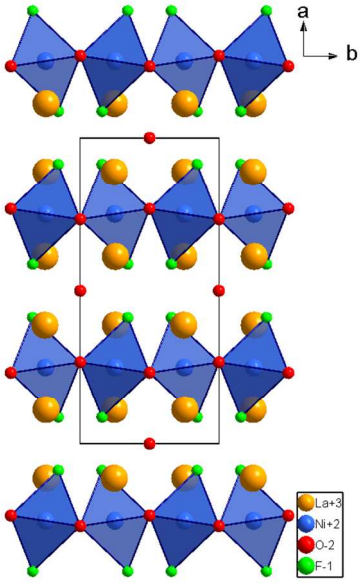

Table of Contents Only: $La_2NiO_3F_2$ crystallizes in a new anion-ordered distortion variant of the n=1 Ruddlesden-Popper type structure. The unprecedented ordering of oxygen anions in the interlayer leads to an expansion of the lattice perpendicular to the stacking direction, accompanied by a strong tilting of NiO_4F_2 octahedra. A weakening of Ni-F-F-Ni superexchange interactions between the perovskite type layers due to the reduced covalency of fluoride ions decreases the magnetic ordering temperature strongly.